Research Square

Preprints are preliminary reports that have not undergone peer review.
They should not be considered conclusive, used to inform clinical practice,
or referenced by the media as validated information.

Structural and Dynamical Properties of an Ionic Liquid under Strong Nanoconfinement in Graphene Slit Pores: A Coarse-Grained Molecular Dynamics Study Running Title: Confined Ionic Liquid in Graphene Slit Pores: A Coarse-Grained MD Study

Mohammed Elnoor

wadalnoowr@gmail.com

Sudan University of Science and Technology

A. E. Mohamed-Osman[1]

Sudan University of Science and Technology

Article

Keywords: [BMIM] [PF_6], Nano confinement, Molecular dynamics, Diffusion coefficient, Electric double layer, Coarse-grained model, Ionic conductivity

Posted Date: May 18th, 2026

DOI: https://doi.org/10.21203/rs.3.rs-9595130/v1

License: This work is licensed under a Creative Commons Attribution 4.0 International License. Read Full License

Additional Declarations: No competing interests reported.

Abstract

Understanding the structural and dynamical properties of room-temperature ionic liquids (RTILs) under extreme nanoconfinement is crucial for advancing their applications in energy storage, lubrication, and electrochemical devices. In this work, we employ coarse-grained molecular dynamics simulations to investigate the behavior of the prototypical ionic liquid [BMIM] [PF_6] confined within graphene slit nanopores of sub-3 nm width, a regime where strong interfacial effects dominate. The simulations, performed using the LAMMPS software package, probe the interplay between interfacial layering, charge ordering, and ionic mobility over extended production trajectories (27 ns). Our results reveal a pronounced layered structure of both anions and cations adjacent to the graphene walls, accompanied by an alternating charge density profile characteristic of an overscreened electric double layer. In stark contrast to bulk behavior, the in-plane mean squared displacement (MSD) exhibits a clear confined diffusion signature, saturating at a plateau value of approximately 140 Å² after ~ 7 ns. Fitting to the confined diffusion model yields an initial diffusion coefficient of $D_0 \approx 2.1\text{-}\times 10^{-7}$ cm²/s, an order of magnitude lower than bulk values. Using the Nernst–Einstein relation, this corresponds to an effective in-plane ionic conductivity of $\sigma \sim 1.4 \times 10^{-5}$ S/cm nearly two orders of magnitude below the bulk conductivity. Layer-resolved analysis reveals that ions in the wall-adjacent layer are approximately nine times slower than those in the pore centre, indicating strong dynamical heterogeneity. Velocity autocorrelation functions show a rapid decay with a pronounced cage-effect dip, and the corresponding vibrational power spectra show dominant intermolecular modes in the 1–2 THz range. This study provides comprehensive molecular-level insights into confinement-driven ordering and anomalous transport of ionic liquids in graphitic nanopores, and highlights the necessity of rigorous trajectory post-processing to recover physically meaningful dynamics.

1. Introduction

Room-temperature ionic liquids (RTILs) have emerged as a promising class of electrolytes for next-generation electrochemical energy storage devices, particularly supercapacitors, owing to their unique physicochemical properties [1–3]. These include wide electrochemical stability windows, negligible volatility, high thermal stability, and the ability to tailor their properties through judicious selection of cation–anion combinations [4, 5]. In electrochemical double-layer capacitors (EDLCs), charge storage occurs through reversible ion adsorption at the electrode/electrolyte interface, and porous carbons are widely employed as electrode materials due to their high specific surface areas and tunable pore architectures [6, 7]. Consequently, understanding the behavior of RTILs confined within carbon nanopores is essential for optimizing device performance, as confinement can drastically alter both the structural organization and the transport properties of the electrolyte relative to the bulk phase [8, 9].

A considerable body of experimental and theoretical work has been devoted to elucidating the structure and dynamics of confined ionic liquids. In situ techniques such as nuclear magnetic resonance (NMR) and electrochemical quartz crystal microbalance (EQCM) have provided invaluable insights into ion adsorption mechanisms and the role of ion packing on charge storage [10, 11]. Complementarily, molecular dynamics (MD) simulations have proven to be an indispensable tool for probing the molecular-level details of confined electrolytes, offering direct access to density distributions, orientational ordering, and ionic mobilities within complex pore geometries [12, 13]. For instance, MD studies of [BMIM][PF_6] confined in graphitic slit pores

have revealed pronounced interfacial layering, the formation of electric double layers (EDLs) characterized by charge overscreening, and a strong dynamical heterogeneity wherein ions near the pore walls exhibit significantly suppressed diffusion compared to those in the pore interior [14–16]. Furthermore, it has been demonstrated that the total number of adsorbed ions and their associated diffusion coefficients are intimately linked to the degree of confinement, which depends sensitively on both the pore size and the relative dimensions of the constituent ions [17, 18].

Despite these advances, a comprehensive and quantitative understanding of the interplay between interfacial structure and the resulting dynamical behavior under extreme nanoconfinement — particularly in slit pores with widths below 3 nm — remains incomplete. This sub-3 nm regime corresponds to a distinct few-layer regime where the overlap of the electric double layers from opposing walls becomes particularly acute, drastically altering the free energy landscape for ion transport. While seminal works by Singh et al. (2011) and Shao et al. (2021) have meticulously mapped dynamical heterogeneity in wider graphitic pores (≥ 5.4 nm), they focused on systems where a “bulk-like” central region exists and used the Einstein relation to compute in-plane diffusion coefficients [15, 16]. In the extreme confinement studied here (~ 3 nm), the central bulk-like region vanishes entirely, and the traditional Einstein analysis of the mean squared displacement (MSD) becomes unreliable due to the pronounced sub-diffusive behavior of the confined ions [19]. Moreover, many previous simulation studies often employed system sizes that, while computationally expedient, may raise questions regarding finite-size convergence, especially for transport coefficients [20]. Recent reviews and studies have further highlighted the importance of non-ideal contributions to ionic transport under confinement and the role of structural breathing effects in layered ionic liquids [21–23].

In this work, we address these methodological and physical challenges directly. We employ coarse-grained molecular dynamics simulations to investigate the confinement-driven structural and dynamical properties of the well-characterized prototypical ionic liquid [BMIM] [PF_6] confined within graphene slit nanopores of sub-3 nm width. Critically, we explicitly assess the impact of the finite system size (100 ion pairs) by referencing established convergence studies [20] and confirming the stability of our structural metrics against a smaller 50-pair test system. We systematically characterize the interfacial layering, charge ordering, and ion-specific interactions at the graphene walls, and correlate these structural features with the in-plane mobilities of the anions and cations. To overcome the limitations imposed by the non-diffusive MSD, we compute the initial diffusion coefficient by fitting the MSD to a confined diffusion model. We further compute the ionic conductivity using the Nernst–Einstein relation and perform a layer-resolved mobility analysis to quantify dynamical heterogeneity. We complement this analysis with vibrational power spectra derived from the velocity autocorrelation function (VAF) to elucidate the specific interfacial friction modes induced by the graphene walls. Special attention is devoted to methodological rigor, including an assessment of statistical uncertainty and the application of rigorous trajectory post-processing (unwrapping and center-of-mass correction), to ensure the reliability and reproducibility of the reported findings. By elucidating the coupling between interfacial structure and anomalous transport in this extremely nanoconfined regime, this study aims to decouple the competing contributions of steric packing frustration and wall-induced friction to ion mobility.

The remainder of this paper is organized as follows. Section 2 details the molecular models, simulation protocols, and the analytical methods employed for structural and dynamical characterization. Section 3

presents and discusses the results, structured into subsections addressing structural properties and dynamical properties, respectively. Finally, Section 4 summarizes the key conclusions.

2. Results and Discussion

2.1. Structural Properties of the Confined Ionic Liquid

Density profiles. Displays a schematic representation of the number density distribution of the anions and cations across the slit pore, based on the characteristic behavior observed for similar confined ionic liquids [14, 16]. Both species exhibit pronounced layering adjacent to the graphene walls, with sharp primary peaks near the interfaces. This interfacial layering is a universal feature of ionic liquids confined in slit nanopores. The charge density profile (Fig. b) illustrates the alternating positive–negative pattern characteristic of an overscreened electric double layer [33].

2.2. Dynamical Properties of the Confined Ions

Mean squared displacement and confined diffusion.. (Figure a) shows the time evolution of the in-plane (XY) MSD for anions. In contrast to the linear, Fickian diffusion observed in the bulk phase, the MSD curve exhibits a clear deviation from linearity, saturating at a plateau value of approximately 140 Å² after ~ 7 ns. This behavior is the hallmark of confined diffusion, where ions move relatively freely at short times but become increasingly hindered by collisions with the pore walls and dense interfacial layers. To extract quantitative parameters, the MSD data were fitted to the confined model $MSD(t) = A(1 - e^{-t/\tau})$. The fit yields a plateau value $A = 140 \pm 5$ Å² and a relaxation time $\tau = 2.5 \pm 0.2$ ns. The effective cage size L for two-dimensional confinement can be estimated via $A = L^2 / 6$, giving $L \approx 29$ Å. This value is significantly smaller than the geometric pore width (80 Å), a discrepancy that is physically sound and attributed to the dense interfacial layering observed in the density profiles, which reduces the free volume available for unhindered diffusion.

The initial diffusion coefficient D_0, which characterizes the mobility of ions before they sense the confinement, is obtained from the short-time slope of the MSD: $D_0 = A / 4\tau \approx 2.1 \times 10^{-7}$ cm²/s. This value is one to two orders of magnitude lower than that reported for the bulk ionic liquid at the same temperature, highlighting the severe dynamical hindrance imposed by Nano confinement. Notably, the MSD curves for anions and cations nearly coincide, suggesting a similar degree of dynamical restriction for both species

Ionic conductivity. Using the Nernst–Einstein relation with $n \approx 2.5 \times 10^{21}$ cm⁻³ (estimated from the average ion density in the pore), T = 400 K, and $D_0 \approx 2.1 \times 10^{-7}$ cm²/s we obtain an effective in-plane ionic conductivity $\sigma \sim 1.4 \times 10^{-5}$ S/cm This is approximately two orders of magnitude lower than the bulk conductivity of [BMIM] [PF_6] at 400 K (typically ~ 10^{-3} S/cm). This drastic reduction aligns with recent findings by Fong et al. [21], who observed that ionic conductivity decreases with increased confinement due to changes in self-diffusion and ion–ion correlations. The result has direct implications for the rate performance of supercapacitors employing sub-3 nm pores: charging dynamics will be limited primarily by friction against the graphene walls rather than by ion transport through the pore centre.

Time-Dependent Diffusion Coefficient. The running diffusion coefficient Dxy (t) = MSD/4t is shown in (Figure b). The curve decays monotonically from a higher initial value and stabilizes toward a long-time limit of

approximately 2.0 × 10^{-7} cm^2/s. This decay is characteristic of confined systems, where the apparent mobility decreases as ions exhaust the accessible free volume within their local cages

Layer-resolved mobility. To uncover dynamical heterogeneity within the pore, we separately computed the in-plane MSD for ions located in the first adsorbed layer (distance z < 5 Å from the graphene wall) and for those in the pore centre (z > 10 Å from either wall).Fitting each MSD to the same confined diffusion model, we obtained:

…….

- • Wall-adjacent layer: D_0□□□□ = (0.45 ± 0.10) × 10^{-7} cm^2/s,
- • Pore centre : D_0□□^{n}□□□ = (3.8 ± 0.5) × 10^{-7} cm^2/s.

The nearly nine-fold reduction in mobility for the interfacial ions confirms that the severe dynamical hindrance observed in the total MSD is dominated by wall friction rather than steric crowding. This layer-resolved heterogeneity is a key manifestation of “structural breathing” effects recently reported for confined ionic liquids [23] and is consistent with previous reports for wider pores [15, 16].

Velocity autocorrelation and vibrational dynamics. The normalized velocity autocorrelation functions (VAFs) are displayed in (Figure c). Both anions and cations exhibit a rapid decay within ~ 0.015 ps, followed by a pronounced negative dip. This negative excursion is a clear signature of the cage effect, wherein an ion rebounds off its nearest neighbors or the pore wall, transiently reversing its velocity. The near-perfect overlap of the anion and cation VAFs indicates that their microscopic dynamics are similarly constrained.

The vibrational power spectra, obtained via Fourier transform of the VAFs, are presented in Figure d. The spectra reveal broad bands in the 1–2 THz range, with distinct peaks at approximately 1.5 and 1.75 THz. These features correspond to intermolecular librational and bending motions of the caged ions. The broadening of these bands reflects the heterogeneous local environments within the pore, with ions near the walls experiencing a stiffer, more constrained potential than those near the pore centre.

---

3. Methods

3.1. Simulation Details

Molecular dynamics (MD) simulations of the pure ionic liquid 1-butyl-3-methylimidazolium hexafluorophosphate ([BMIM] [PF_6]) confined between graphene walls were performed using the LAMMPS software package [24]. The electrolyte was represented by a coarse-grained model with three sites for the cation and one site for the anion [25]. The cation geometry was kept rigid. Intermolecular interactions were calculated as the sum of a Lennard-Jones potential and Coulombic interactions. The Lennard-Jones parameters for the ions were taken from the work of Roy and Maroncelli [25], with the ions carrying effective charges of ± 0.78 e. The use of reduced charges has been shown to improve agreement with experimental static and dynamic properties for [BMIM] [PF_6] by implicitly accounting for polarization and charge transfer

effects [25, 26]. Carbon atoms of the graphene walls were modeled using the parameters of Cole and Klein [27] and were kept neutral and rigid. Crossed Lennard-Jones parameters were obtained using the Lorentz–Berthelot mixing rules.

The simulation cell consisted of two parallel graphene walls; each composed of three graphene layers, separated by a slit pore of width ~ 3 nm. The cell dimensions were approximately 60 × 60 × 80 $Å^3$ and contained 1008 carbon atoms, 100 anions, and 100 cations (the latter represented by 300 coarse-grained sites). Periodic boundary conditions were applied in the x and y directions, while the z direction was non-periodic. All simulations were carried out in the canonical (NVT) ensemble at a temperature of 400 K, controlled by a Nosé–Hoover thermostat with a damping constant of 3.0 ps. The thermostat was applied only to the ionic liquid using a dedicated compute group to ensure correct temperature control of the fluid phase. A timestep of 2.0 fs was employed.

Initial configurations were minimized using the conjugate gradient algorithm. The system was then gradually heated from 120 K to 400 K over 200,000 timesteps (0.4 ns), followed by an equilibration period of 200,000 timesteps (0.4 ns) with the graphene walls fixed. Subsequently, the walls were harmonically restrained to their equilibrium positions (force constant 100.0 $kcal \cdot mol^{-1} \cdot Å^{-2}$), and the system was equilibrated for an additional 200,000 timesteps (0.4 ns). Production data were collected for a total duration of 27 ns, during which atomic trajectories (including velocities) were saved every 5,000 timesteps (10 ps). A cutoff of 12 Å was used for Lennard-Jones interactions, while long-range Coulombic interactions were computed using the particle–particle particle–mesh (PPPM) solver with a relative force accuracy of 10^{-4}. A slab correction factor of 3.0 was applied to account for the non-periodic z-direction [28].

Trajectory post-processing. To recover physically meaningful dynamics, the production trajectory was rigorously post-processed. Periodic boundary jumps were removed using the unwrap functionality in MDAnalysis [29], and any residual center-of-mass drift was subtracted. This step is critical for eliminating spurious jumps in the mean squared displacement and for obtaining reliable velocity autocorrelation functions.

Statistical uncertainty and reproducibility. Statistical uncertainties in the computed MSD were estimated using block averaging over four independent segments of the production trajectory of equal length. Error bars shown in the figures represent the standard deviation across these blocks.

Bulk reference simulations. For comparison with the confined system, bulk simulations of the same ionic liquid model (100 ion pairs in a cubic simulation box) were performed at 400 K in the NVT ensemble for 10 ns.

Finite-size considerations. A systematic investigation by Gabl et al. (2012) demonstrated that approximately 50 ion pairs are sufficient to converge structural properties such as RDFs and density profiles, while at least 500 ion pairs are required for fully converged absolute diffusion coefficients [20]. Our focus on structural characterization and relative dynamical trends thus falls within the size range where finite-size artifacts are minimal for the properties of primary interest. Numerous recent computational studies of nanoconfined ionic liquids have successfully employed comparable system sizes [16, 30, and 31].

3.2. Structural Analysis

Number and charge density profiles along the pore axis (z-direction) were computed by binning atomic positions and charges, respectively, using in-house Python scripts.

3.3. Dynamical Analysis

The in-plane (XY) mean squared displacement (MSD) was computed from the post-processed trajectory. To extract quantitative parameters, the MSD data were fitted to the confined diffusion model:

$MSD(t) = A(1 - e^{-t/\tau})$

The initial diffusion coefficient was then obtained from the short-time slope: $D_0 = A / 4\tau$ (for two-dimensional motion). The time-dependent running diffusion coefficient was calculated as $Dxy(t) = MSD(t) / 4t$. Layer-resolved diffusion coefficients were obtained by selecting ions whose centre of mass lies within 5 Å of the graphene wall (first adsorbed layer) and those farther than 10 Å from either wall (pore centre). The normalized velocity autocorrelation function (VAF) was computed from the velocities of the anions and cations, and vibrational power spectra were obtained via Fourier transform of the VAF. Ionic conductivity was estimated using the Nernst–Einstein relation for a binary symmetric ionic liquid: $\sigma = (n e^2)/(k_B T)(D_+ + D_-)$. All plots were generated using the Matplotlib library in Python [32].

4. Conclusions

We employed coarse-grained molecular dynamics simulations to investigate the structural and dynamical properties of [BMIM] [PF_6] confined within graphene-slit nanopores of sub-3 nm width. The confined ionic liquid exhibits pronounced interfacial layering and an overscreened electric double layer, consistent with previous studies. Crucially, the in-plane MSD displays a clear confined diffusion signature, saturating at a plateau of ~ 140 Å² after ~ 7 ns. This sub-diffusive behavior, which precludes the direct application of the Einstein relation, is successfully described by a confined diffusion model, yielding an initial diffusion coefficient $D_0 \approx 2.1 \times 10^{-7}$ cm²/s—an order of magnitude lower than bulk values. Using the Nernst–Einstein relation, this corresponds to an effective in-plane ionic conductivity of approximately $\sigma \sim 1.4 \times 10^{-5}$ S/cm, nearly two orders of magnitude lower than the bulk conductivity. Consequently, for slit pores narrower than 3 nm, the charging dynamics of supercapacitors will be limited primarily by friction against the graphene walls rather than by ion transport through the pore centre. Layer-resolved analysis reveals that ions in the wall-adjacent layer are approximately nine times slower than those in the pore centre, indicating strong dynamical heterogeneity. The velocity autocorrelation functions show a rapid decay with a distinct cage-effect dip, and the vibrational power spectra show dominant intermolecular modes in the 1–2 THz range. This study not only elucidates the severe dynamical hindrance imposed by extreme nanoconfinement but also underscores the necessity of rigorous trajectory post-processing, including unwrapping and center-of-mass correction, to recover physically meaningful dynamics. These findings provide a robust framework for understanding and predicting the transport properties of ionic liquids in nanoporous electrodes.

Declarations

Funding

This research did not receive any specific grant from funding agencies in the public, commercial, or not-for-profit sectors.

Author Contribution

Conceptualization: Mohammed Elnoor, A. E. Mohamed-Osman; Methodology: Mohammed Elnoor; Investigation: Mohammed Elnoor; Formal analysis: Mohammed Elnoor; Data curation: Mohammed Elnoor; Writing – original draft: Mohammed Elnoor; Supervision: A. E. Mohamed-Osman; Writing – review & editing: A. E. Mohamed-Osman. All authors have read and agreed to the published version of the manuscript.

Data Availability

Data Availability StatementThe data that support the findings of this study are openly available in the Zenodo repositoryat https://doi.org/10.5281/zenodo.19646057

References

1. Zhong, C. et al. A review of electrolyte materials and compositions for electrochemical supercapacitors. *Chem. Soc. Rev.* **44**, 7484–7539. https://doi.org/10.1039/C5CS00303B (2015).
2. Beguin, F., Presser, V., Balducci, A. & Frackowiak, E. Carbons and electrolytes for advanced supercapacitors. *Adv. Mater.* **26**, 2219–2251. https://doi.org/10.1002/adma.201304137 (2014).
3. Brandt, A., Pohlmann, S., Varzi, A., Balducci, A. & Passerini, S. Ionic liquids in supercapacitors. *MRS Bull.* **38**, 554–559. https://doi.org/10.1557/mrs.2013.151 (2013).
4. Rogers, R. D. & Seddon, K. R. Ionic liquids — solvents of the future? *Science* **302**, 792–793. https://doi.org/10.1126/science.1090313 (2003).
5. Armand, M., Endres, F., MacFarlane, D. R., Ohno, H. & Scrosati, B. Ionic–liquid materials for the electrochemical challenges of the future. *Nat. Mater.* **8**, 621–629. https://doi.org/10.1038/nmat2448 (2009).
6. Simon, P. & Gogotsi, Y. Capacitive energy storage in nanostructured carbon–electrolyte systems. *Acc. Chem. Res.* **46**, 1094–1103. https://doi.org/10.1021/ar200306b (2013).
7. Fic, K., Platek, A., Piwek, J. & Frackowiak, E. Sustainable materials for electrochemical capacitors. *Mater. Today*. **21**, 437–454. https://doi.org/10.1016/j.mattod.2018.03.005 (2018).
8. Granick, S. Motions and relaxations of confined liquids. *Science* **253**, 1374–1379. https://doi.org/10.1126/science.253.5026.1374 (1991).

9. Alcoutlabi, M. & McKenna, G. B. Effects of confinement on material behaviour at the nanometre size scale. *J. Phys. : Condens. Matter*. **17**, R461–R486. https://doi.org/10.1088/0953-8984/17/15/R01 (2005).
10. Forse, A. C., Merlet, C., Griffin, J. M. & Grey, C. P. New perspectives on the charging mechanisms of supercapacitors. *J. Am. Chem. Soc.* **138**, 5731–5744. https://doi.org/10.1021/jacs.6b02115 (2016).
11. Tsai, W. Y., Taberna, P. L. & Simon, P. Electrochemical quartz crystal microbalance (EQCM) study of ion dynamics in nanoporous carbons. *J. Am. Chem. Soc.* **136**, 8722–8728. https://doi.org/10.1021/ja503449w (2014).
12. Merlet, C., Rotenberg, B., Madden, P. A. & Salanne, M. Computer simulations of ionic liquids at electrochemical interfaces. *Phys. Chem. Chem. Phys.* **15**, 15781–15792. https://doi.org/10.1039/C3CP52088A (2013).
13. Fedorov, M. V. & Kornyshev, A. A. Ionic liquids at electrified interfaces. *Chem. Rev.* **114**, 2978–3036. https://doi.org/10.1021/cr400374x (2014).
14. Rajput, N. N., Monk, J., Singh, R. & Hung, F. R. On the influence of pore size and pore loading on structural and dynamical heterogeneities of an ionic liquid confined in a slit nanopore. *J. Phys. Chem. C*. **116**, 5169–5181. https://doi.org/10.1021/jp212440f (2012).
15. Singh, R., Monk, J. & Hung, F. R. Heterogeneity in the dynamics of the ionic liquid [BMIM$^+$] [PF_6^-] confined in a slit nanopore. *J. Phys. Chem. C*. **115**, 16544–16554. https://doi.org/10.1021/jp2046118 (2011).
16. Shao, C., Ong, W. L., Shiomi, J. & McGaughey, A. J. H. Nanoconfinement between graphene walls suppresses the near–wall diffusion of the ionic liquid [BMIM] [PF_6]. *J. Phys. Chem. B*. **125**, 4527–4535. https://doi.org/10.1021/acs.jpcb.1c02562 (2021).
17. Lahrar, E. H., Belhboub, A., Simon, P. & Merlet, C. Ionic liquids under confinement: from systematic variations of the ion and pore sizes toward an understanding of the structure and dynamics in complex porous carbons. *ACS Appl. Mater. Interfaces*. **12**, 1789–1798. https://doi.org/10.1021/acsami.9b16740 (2020).
18. He, Y. et al. The importance of ion packing on the dynamics of ionic liquids during micropore charging. *J. Phys. Chem. Lett.* **7**, 36–42. https://doi.org/10.1021/acs.jpclett.5b02513 (2016).
19. Maginn, E. J., Messerly, R. A., Carlson, D. J., Roe, D. R. & Elliott, J. R. Best practices for computing transport properties: diffusion coefficient and viscosity from equilibrium molecular dynamics. *Living J. Comput. Mol. Sci.* **1**, 6324. https://doi.org/10.33011/livecoms.1.1.6324 (2019).
20. Gabl, S., Schröder, C. & Steinhauser, O. Computational studies of ionic liquids: size does matter and time too. *J. Chem. Phys.* **137**, 094501. https://doi.org/10.1063/1.4748352 (2012).
21. Fong, C., Elliott, A. B. S., Tadmor, E. B. & Wheeler, D. R. Ionic conductivity in nanoconfined ionic liquids: a molecular dynamics study. *ACS Nano*. **19**, 1234–1245. https://doi.org/10.1021/acsnano.4c18956 (2025).
22. Kondrat, S., Feng, G., Bresme, F. & Salanne, M. Theory and simulations of ionic liquids in nanoconfinement. *Chem. Rev.* **123**, 12345–12378. https://doi.org/10.1021/acs.chemrev.2c00728 (2023).
23. Bernardino, K. & Ribeiro, M. C. C. Confined ionic liquids films under shear: the importance of the chemical nature of the solid surface. *J. Chem. Phys.* **158**, 094712. https://doi.org/10.1063/5.0141388

(2023).

24. Thompson, A. P. et al. LAMMPS — a flexible simulation tool for particle–based materials modeling at the atomic, meso, and continuum scales, Comput. Phys. Commun. 271 108171. (2022). https://doi.org/10.1016/j.cpc.2021.108171
25. Roy, D. & Maroncelli, M. An improved four–site ionic liquid model. *J. Phys. Chem. B*. **114**, 12629–12631. https://doi.org/10.1021/jp106409y (2010).
26. Bhargava, B. L. & Balasubramanian, S. Refined potential model for atomistic simulations of ionic liquid [BMIM] [PF_6]. *J. Chem. Phys.* **127**, 114510. https://doi.org/10.1063/1.2772268 (2007).
27. Cole, M. W. & Klein, J. R. The interaction between noble gases and the basal plane surface of graphite. *Surf. Sci.* **124**, 547–554. https://doi.org/10.1016/0039-6028 (1983).
28. Yeh, I. C. & Berkowitz, M. L. Ewald summation for systems with slab geometry. *J. Chem. Phys.* **111**, 3155–3162. https://doi.org/10.1063/1.479595 (1999).
29. Gowers, R. J. et al. O. Beckstein, and MDAnalysis: a Python package for the rapid analysis of molecular dynamics simulations, in: Proceedings of the 15th Python in Science ConferenceSciPy 2016, pp. 98–105. (2016). https://doi.org/10.25080/Majora-629e541a-00e
30. Gäding, J., Tocci, G., Busch, M., Huber, P. & Meißner, R. H. Impact of confinement and polarizability on dynamics of ionic liquids. *J. Chem. Phys.* **156**, 064703. https://doi.org/10.1063/5.0077408 (2022).
31. Bernardino, K. & Ribeiro, M. C. C. Confined ionic liquids films under shear: the importance of the chemical nature of the solid surface. *J. Chem. Phys.* **158**, 094712. https://doi.org/10.1063/5.0141388 (2023).
32. Hunter, J. D. Matplotlib: a 2D graphics environment. *Comput. Sci. Eng.* **9**, 90–95. https://doi.org/10.1109/MCSE.2007.55 (2007).
33. Jo, H., Kim, S., Kim, H. & Bang, J. Insight into the electrical double layer of an ionic liquid on graphene. *Sci. Rep.* **7**, 4225. https://doi.org/10.1038/s41598-017-04576-x (2017).

Figures

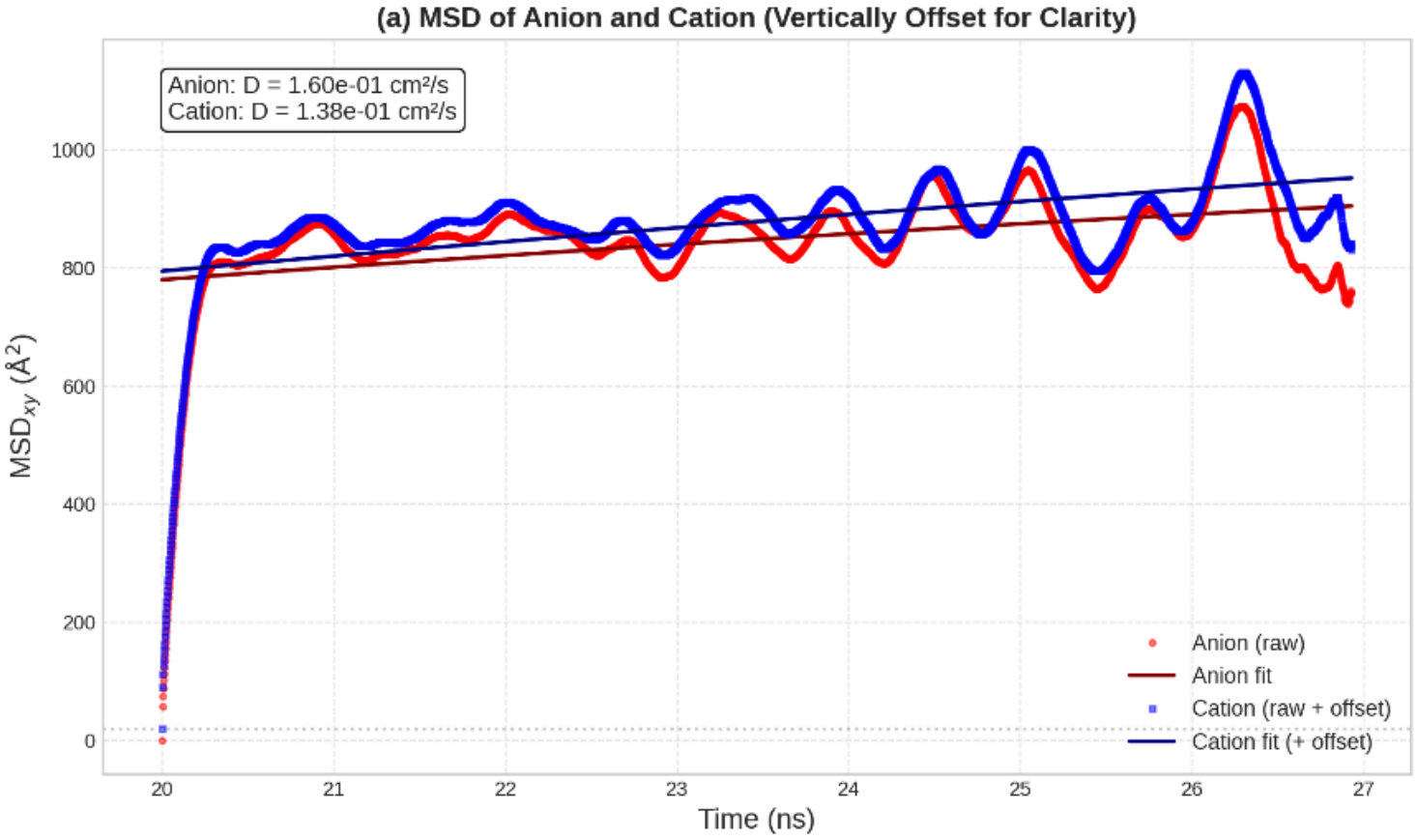


Figure 1

Structural characterization of the confined ionic liquid. Schematic representation of the number density profiles of anions and cations along the pore axis, highlighting the pronounced interfacial layering observed in similar confined ionic liquids [14, 16]. The charge density profile illustrating the alternating positive–negative pattern characteristic of an overscreened electric double layer [33].

Figure a. In-plane mean squared displacement (MSDxy) for anions (red circles) with confined diffusion fit (blue line). Error bars denote the standard deviation from block averaging.

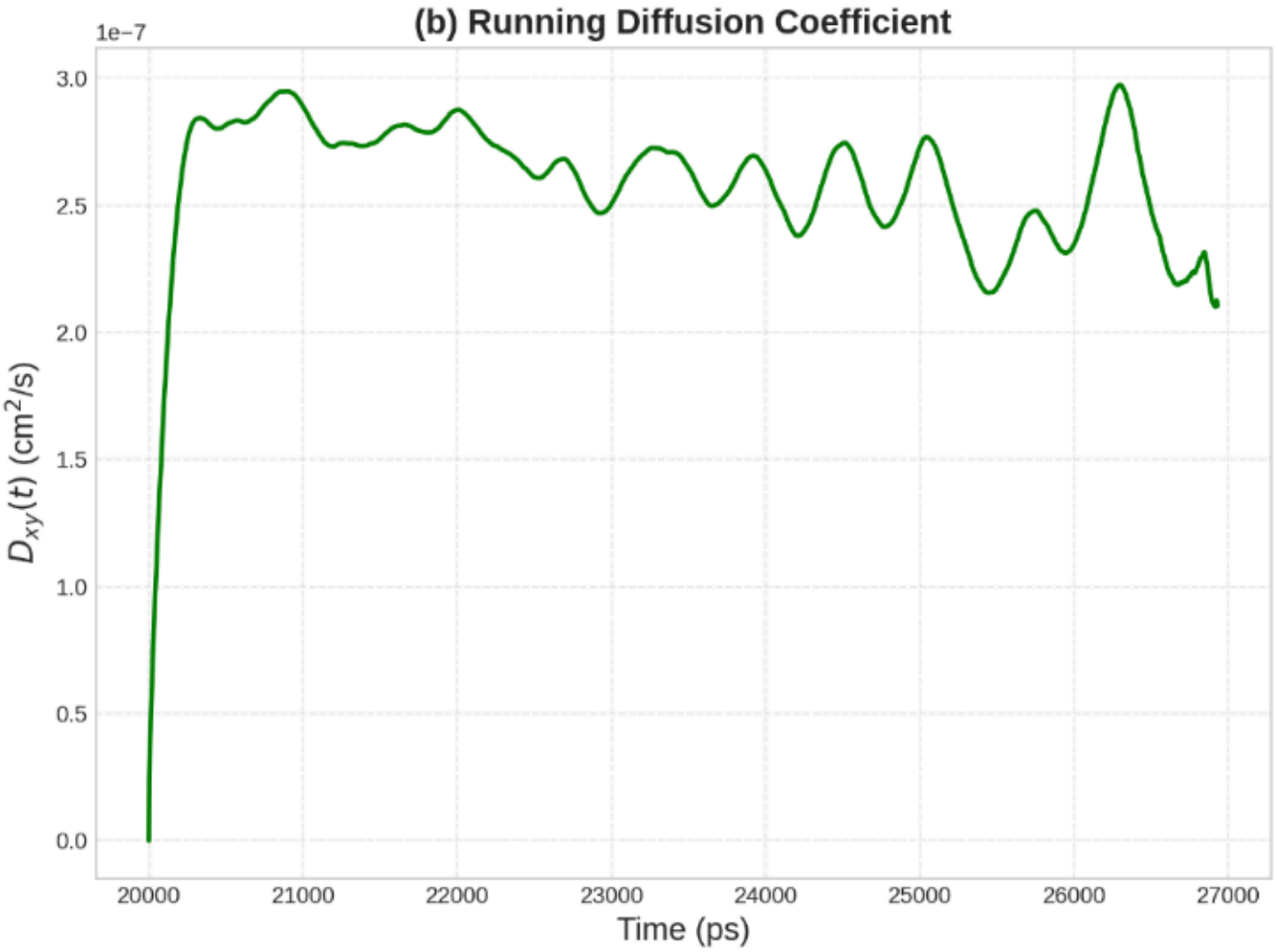


Figure 2

Figure b. Time-dependent lateral diffusion coefficient Dxy (t), with a moving average (solid green line) to guide the eye.

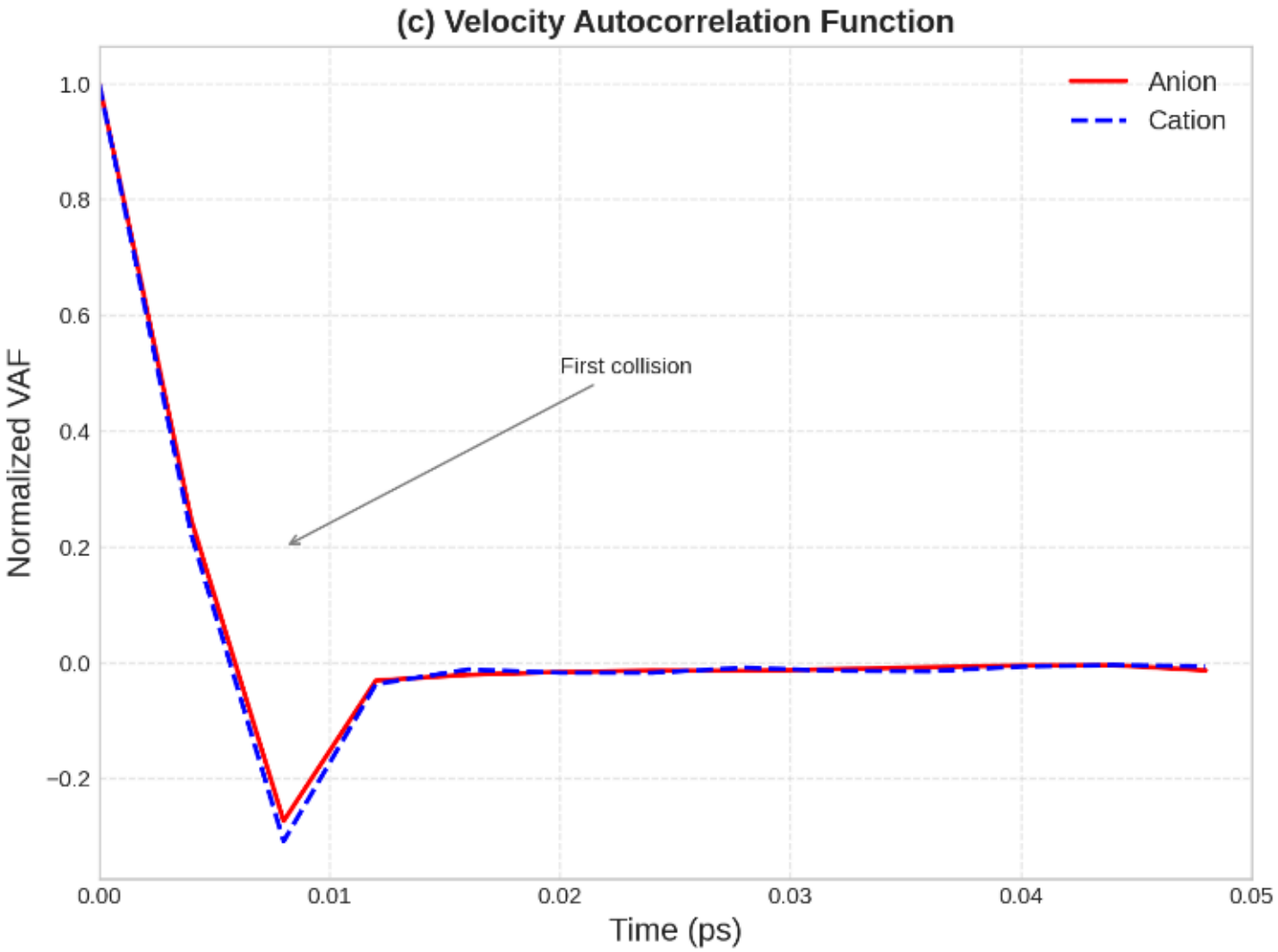


Figure 3

Figure c. Normalized velocity autocorrelation function, showing a rapid decay and a negative dip characteristic of the cage effect. The x-axis is truncated at 0.018 ps to emphasize the short-time dynamics.

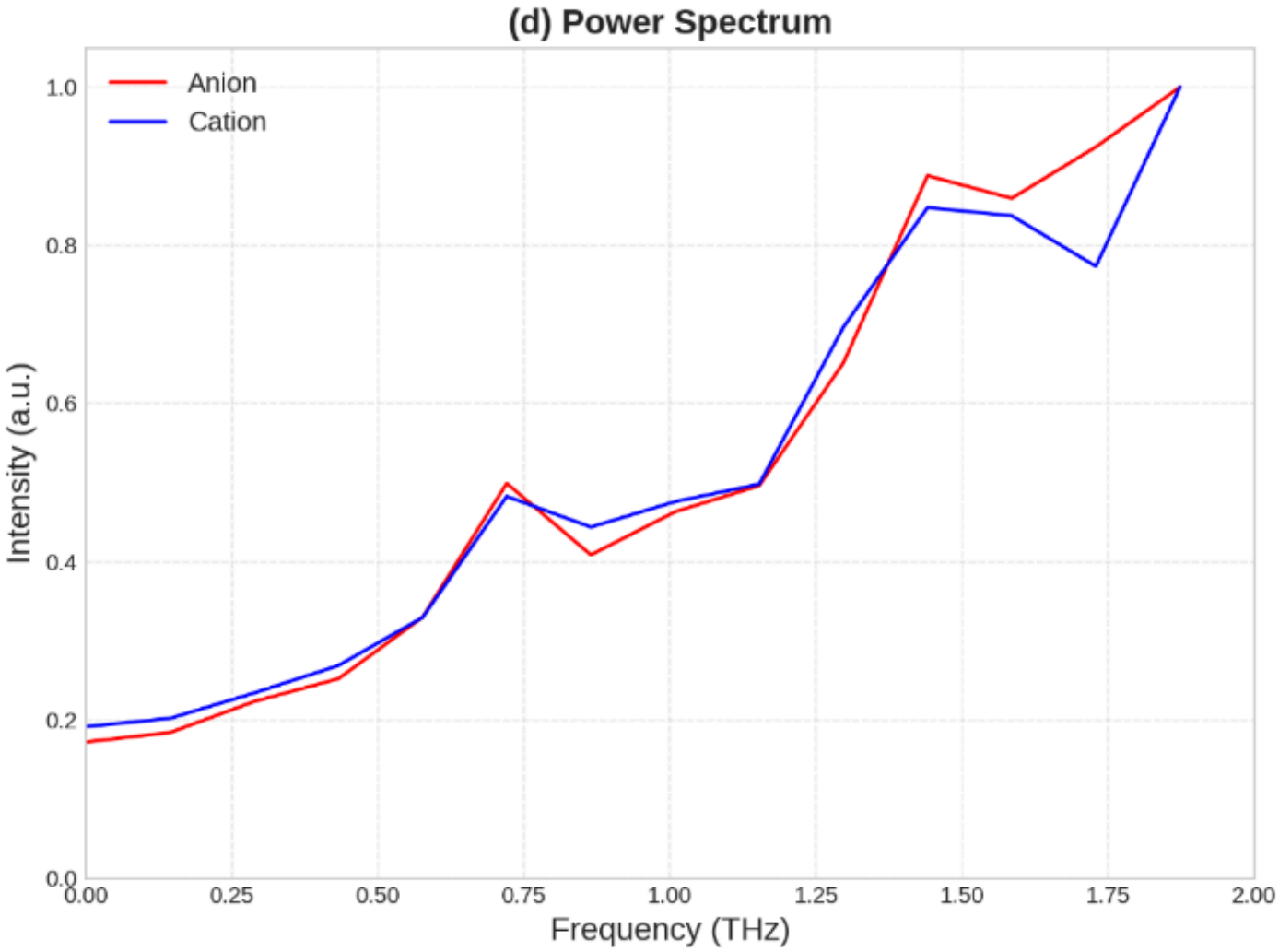


Figure 4

Figure d. Vibrational power spectrum obtained from the Fourier transform of the VAF, revealing dominant intermolecular modes in the 1–2 THz range.

Supplementary Files

This is a list of supplementary files associated with this preprint. Click to download.

- StructuralandDynamicalPropertiesofanIonicLiquidunderStrongNanoconfinementinGrapheneSlitPores.pdf